Interannual variability of nitrogen oxides emissions from boreal fires in Siberia and Alaska during 1996–2011 as observed from space

2015 Environ. Res. Lett. 10 065004

(http://iopscience.iop.org/1748-9326/10/6/065004)

Environmental Research Letters

LETTER

Interannual variability of nitrogen oxides emissions from boreal fires in Siberia and Alaska during 1996–2011 as observed from space

Hiroshi Tanimoto[1], **Kohei Ikeda**[1], **K Folkert Boersma**[2,3], **Ronald J van der A**[3] **and Savitri Garivait**[4]

[1] Center for Global Environmental Research, National Institute for Environmental Studies, Tsukuba, Japan
[2] Meteorology and Air Quality Group, Wageningen University, Wageningen, The Netherlands
[3] Climate Observations Department, Royal Netherlands Meteorological Institute (KNMI), De Bilt, The Netherlands
[4] The Joint Graduate School of Energy and Environment (JGSEE), King Mongkut's University of Technology Thonburi, Bangkok, Thailand

E-mail: tanimoto@nies.go.jp, folkert.boersma@wur.nl, avander@knmi.nl and savitri_g@jgsee.kmutt.ac.th

OPEN ACCESS

RECEIVED
18 January 2015

REVISED
22 April 2015

ACCEPTED FOR PUBLICATION
22 April 2015

PUBLISHED
2 June 2015

Keywords: nitrogen oxides, boreal fires, emission, Siberia, Alaska

Supplementary material for this article is available online

Abstract

Past studies suggest that forest fires contribute significantly to the formation of ozone in the troposphere. However, the emissions of ozone precursors from wildfires, and the mechanisms involved in ozone production from boreal fires, are very complicated. Moreover, an evaluation of the role of forest fires is prevented by the lack of direct observations of the ozone precursor, nitrogen oxides (NO*x*), and large uncertainties exist in the emissions inventories currently used for modelling. A comprehensive understanding of the important processes and factors involving wildfires has thus been unobtainable. We made 16 year consistent analyses of NO*x* emissions from boreal wildfires by using satellite observations of tropospheric nitrogen dioxides (NO_2) from 1996 to 2011. We report substantial interannual variability of tropospheric NO_2 originating from large boreal fires over Siberia in 1998, 2002, 2003, 2006, and 2008; and over Alaska in 2004, 2005, and 2009. Monthly comparisons of NO_2 enhancements with fire radiative power (FRP) show reasonably strong correlation, suggesting that FRP is a better proxy than burned area for boreal fire NO*x* emissions. We provide space-based constraints on NO*x* emission factors (EFs) for Siberian and Alaskan fires. Although the associated uncertainty is relatively large, the derived EFs fall into a in reasonably agreeable range with those previously determined by *in situ* ground-based and airborne observations over these regions.

1. Introduction

Biomass burning plays an important role in the Earth's climate system and global biogeochemical cycles, and wildfires in boreal regions such as Siberia and Alaska are important sources of trace gases and aerosols emitted into the atmosphere. In the atmosphere, nitrogen oxides (NO*x*) and non-methane volatile organic compounds (NMVOCs) emitted from fires are subject to photochemical oxidation, affecting the oxidizing capacity and radiative budget of the atmosphere by serving as precursors of tropospheric ozone (O_3). Although it is generally believed that biomass burning is a substantial contributor to tropospheric O_3 production, observational evidence during the past decades has shown contradicting pictures, suggesting that the emissions of O_3 precursors from wildfires, and the mechanisms involved in O_3 production from boreal fires, are very complicated and nonlinear. For example, plume chemistry is not often resolved, injection height is often not known, and chemical interference of the emitted gases with aerosols in the plume can alter photolysis rates and provide heterogeneous surfaces.

The emission and long-range transport of carbon monoxide (CO) from fires has been well studied, both in terms of pollution episodes and interannual variability (e.g., Tanimoto *et al* 2000, 2009, Yurganov *et al* 2004, 2005, 2010, Turquety *et al* 2007). The enhancement of CO from fire emissions is identifiable due to its relatively long lifetime, and it is known that Siberian and Alaskan fires contribute substantially to

the global CO budget (van der Werf *et al* 2010, van Leeuwen and van der Werf 2011). However, in contrast to CO, the impact from boreal fires on O_3 has been less well quantified, in spite of its potentially important role in controlling day-to-day variations, interannual variability, and long-term trends of tropospheric O_3.

The episodic enhancement of O_3 relative to CO in boreal fire plumes has been examined in several observations, with diverse results ranging from negative to positive O_3 production (e.g., Tanimoto *et al* 2000, 2008, Jaffe *et al* 2004). The magnitude of O_3 enhancement in biomass burning plumes is a recent topic of discussion (Jaffe and Wigder 2012). Identifying the impact on O_3 interannual variability is also challenging, as it is only in the range of 0–5 ppbv (Tanimoto 2009). Thus, investigations relating to tropospheric O_3 are considerably more complicated than those pertaining to CO, because O_3 production depends on various factors including fire emissions, photochemical reactions, meteorology, and aerosol effects.

One of the major constraints to O_3 production is the availability of NO*x* emitted from primary sources, as NO*x* is a key precursor for O_3 production. However, the levels, variability, and distribution of NO*x* near fire regions have not been extensively examined, because measurements are generally not conducted near fires, and measurements made at remote downwind sites are of limited use due to the short lifetime of NO*x*. In addition, measurements of NO*x* are not widely available from operational monitoring networks. Thus, the understanding of NO*x* emissions from fires has been limited. Investigations using satellite NO_2 observations to analyse changes in NO*x* emissions have been reported for a variety of emission sources, mainly from anthropogenic sources (e.g., Ghude *et al* 2008, Castellanos and Boersma 2012, Miyazaki *et al* 2012) and from soil (Ghude *et al* 2010, Hudman *et al* 2010). Several studies have recently explored biomass burning sources, including wildfires in Western North America (Mebust *et al* 2011), in Western Siberia near Moscow in 2010 (Huijnen *et al* 2012), and in South America (Castellanos *et al* 2014), and these studies have focused on the contribution of relatively intensive burning to emissions of NO*x*. In addition, global-scale biomass burning emissions of NO*x* from steadily burning areas have very recently been reported in terms of climatological emissions, for 2005–2011 using an Ozone Monitoring Instrument (OMI) (Mebust and Cohen 2014) and for 2007–2011 using the Global Ozone Monitoring Experiment-2 (GOME-2) and OMI sensors (Schreier *et al* 2014). However, detailed information, such as seasonal and interannual variability, has not yet been studied, especially not on the 16 year timescale as done here. In particular, the variability of NO*x* emissions due to wildfires in boreal regions has not been examined, even though it is expected to be substantial.

In general, interannual variability in tropospheric NO_2 columns is small compared to multi-year trends driven by anthropogenic emissions (e.g., Richter *et al* 2005, Van der A *et al* 2008, Hilboll *et al* 2013). In this study, we examined polar-orbiting satellite NO_2 observations over boreal forests, where data to constrain biomass burning emissions has been lacking relative to other ecological regions, while the contribution of fires to atmospheric chemistry is likely larger due to sparse population, and the sensitivity to climate change is higher relative to mid-latitude ecosystems. We found that satellite instruments are capable of detecting interannual variability of tropospheric NO_2 over Siberia and Alaska for the period 1996–2011. Enhancements noted therein were attributed to NO*x* emissions from forest fires. A systematic examination of the NO*x* emission coefficient due to wildfires was then conducted, with a particular emphasis on the years with strong fire activity (hereafter referred to as 'large-fire years') of 2002, 2003, 2006, and 2008 for Siberia; and 2004, 2005, and 2009 for Alaska. Analysis of tropospheric NO_2 enhancements with fire radiative power (FRP) revealed reasonable correlations, suggesting that fire energy is a good proxy for NO*x* emissions from boreal fires.

2. Satellite observations and emissions inventory

We used robust and consistent long-term records of polar-orbital satellite data from the GOME and SCanning Imaging Absorption spectroMeter for Atmospheric CartograpHY (SCIAMACHY) sensors on-board the ERS-2 and Envisat platforms, respectively. Both spectrometers are nadir-viewing, measuring backscattered light from the Earth's atmosphere in the ultraviolet and visible wavelength range. The GOME observations provide a ground pixel size of 40×320 km^2 and equatorial overpasses at 10:30 LT. Data are available since 1995, with global coverage every 3 days. SCIAMACHY has been observing the atmosphere since 2002, in alternating limb and nadir directions, and nadir observations only are used for tropospheric NO_2 retrieval, resulting in global coverage every 6 days. Data frequency is improved at high latitudes. For example, it takes 2–3 days to achieve complete coverage at 60°N. The SCIAMACHY observations provide a ground pixel size of 30×60 km^2, and an equatorial overpass time at 10:00 LT. The updated product of the retrieval algorithm (version 2.0) was used, and is publicly available on the TEMIS project website (www.temis.nl). This product was evaluated for detailed error estimates and kernel information, as reported in Boersma *et al* (2004, 2011). Only observations with a top-of-atmosphere radiance fraction of less than 50% from clouds (and aerosols) were used. We used the monthly means of tropospheric NO_2 column data with a horizontal resolution of

0.25° × 0.25° from 1996 to 2011. Daily satellite data have been interpolated onto a 0.25° × 0.25° grid with the individual pixel's fractional coverage of the grid cell as a weight in the subsequent calculation of the monthly average. GOME and SCIAMACHY data overlapped for the period from August 2002 to June 2003. For a detailed comparison to FRP, the 0.25° × 0.25° data set was re-gridded to a 1° × 1° resolution.

We also used satellite data from the MODerate resolution Imaging Spectroradiometers (MODIS) on board NASA's Terra satellite launched in December 1999, which have corresponding equatorial overpass times of 10:30 LT. MODIS data from the Aqua satellite was not utilized because the overpass time is 13:30 LT, which does not match with GOME or SCIAMACHY, and data is not available before 2002. The MODIS instrument has 36 spectral bands ranging in wavelength from 0.4 to 14.4 μm. Differences in 4 and 11 μm black body radiation emitted at combustion temperatures were used to locate active fires at a horizontal resolution of 1 km^2. The 'MOD14CM1.005' product was also used, which is available at a horizontal resolution of 1° × 1°, to examine FRP as a proxy of the radiant component of energy release from fires (Kaufman *et al* 1998, Justice *et al* 2002).

The third satellite-based product used was the Global Fire Emissions database (GFED), which relies on improved MODIS-derived estimates of areas burned (or burned scars), fire activity, and plant productivity, and a revised version of the Carnegie–Ames–Stanford-Approach biogeochemical model. To calculate emissions of trace gases and aerosols, emission factors (EFs) were applied based on the studies of Andreae and Merlet (2001) or Akagi *et al* (2011). The GFED version 3 data set, with a horizontal resolution of 0.5° × 0.5°, has been available since 1997 (http://globalfiredata.org/). Updates from version 2 include improved satellite input data, explicitly accounting for deforestation and forest degradation fires in the model, partitioning fire emissions into different source categories, and adding an uncertainty analysis (van der Werf *et al* 2010). Monthly data re-gridded to a 1° × 1° resolution was used to match with the horizontal resolution of FRP.

3. Results

A systematic examination of boreal fires occurring in Siberia and Alaska was made for the period 1996–2011. Figure 1 shows the 15 year time series of regional mean NO*x* emissions as calculated by GFEDv3 and FRP, for Siberia and Alaska, throughout the period 1996–2011. We focused on the regions of Eastern Siberia (48–65°N, 98–142°E) and the entire area of Alaska (60–70°N, 160–120°W) to eliminate possible influences from anthropogenic NO*x* emissions in more densely populated areas in Western and Central Siberia, and in Canada. GFEDv3 predicted large NO*x* emissions from Siberian fires in 1998, 2002, 2003, 2006, and 2008, while the emissions were also significant in other years during the spring–summer seasons (April–October). This was in accordance with previous papers reporting the emissions of trace gases and aerosols from Siberian fires (Yurganov *et al* 2010). The time-series of FRP shows clear seasonal cycles from the year 2001. Similar to the results from GFEDv3, the seasonality of FRP indicates burning in warm seasons in spring and summer, but also extends to cold seasons; results yield broader peaks than GFEDv3. The interannual variability of the magnitude of FRP is generally similar to that of GFEDv3; for example, high FRP is indicated in 2003 and 2008. However, the contrast between large-fire years and small-fire years is not as large as that of GFEDv3.

For Alaska, GFEDv3 predicts large NO*x* emissions from fires in 2004, 2005, and 2009, but considerably less emissions in other years during summer seasons (May–August). The burning period in Alaska is much shorter than that of Siberia. Emissions of trace gases and aerosols from Alaskan fires in these years have been previously reported (Turquety *et al* 2007). The time-series of FRP shows clear seasonal cycles, and indicates high FRP in 2004, 2005, and 2009. It is interesting to note that the agreement between FRP and GFEDv3 is much better for Alaska than for Siberia, and the burning period predicted by FRP is the same that of GFEDv3. Overall, the seasonal and interannual contrasts between large-fire years and small-fire years are in good agreement. In this analysis, we focus on the large-fire years of 2002, 2003, 2006, and 2008 for Siberia; and 2004, 2005, and 2009 for Alaska.

The seasonality of 'baseline' tropospheric NO_2 columns over Siberia and Alaska was examined by calculating the climatological means from small-fire years. For Siberia, we calculated the 11 year climatology from 1996, 1997, 1999, 2000, 2001, 2004, 2005, 2007, 2009, 2010, and 2011, when fire events were minor relative to the large-fire years of 1998, 2002, 2003, 2006, and 2008. Similarly, for Alaska, we calculated the 13 year climatology from 1996, 1997, 1998, 1999, 2000, 2001, 2002, 2003, 2006, 2007, 2008, 2010, and 2011. Wintertime data (from December to March) for Alaska were neglected because of the insufficient amount of data (less than 1000 pixels) available over high latitudes in boreal winter due to no light. Regional mean tropospheric NO_2 columns over Siberia were in the range from 0.6 to 1.2×10^{15} molecules cm^{-2} over the course of year, and were associated with substantial seasonal variations, showing a summer minimum and winter maximum, reflecting the varying lifetime of NO_2 in the troposphere. The levels of baseline mean tropospheric NO_2 columns over Alaska in summer were in the range of $0.4–0.6 \times 10^{15}$ molecules cm^{-2}, which was slightly lower than, but close to, those over Siberia in summer. The levels in other months were lower than over Siberia, resulting in overall negligible seasonal features.

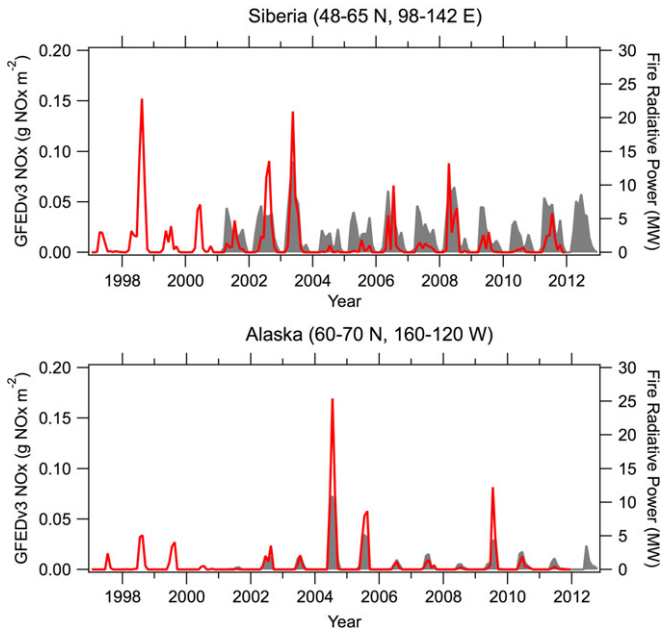

Figure 1. Fifteen year time series (1996–2011) of regional mean NO*x* emissions calculated by GFEDv3 (red lines, left axis), and fire radiative power (grey areas, right axis) for Siberia (48–65°N, 98–142°E) and Alaska (60–70°N, 160–120°W).

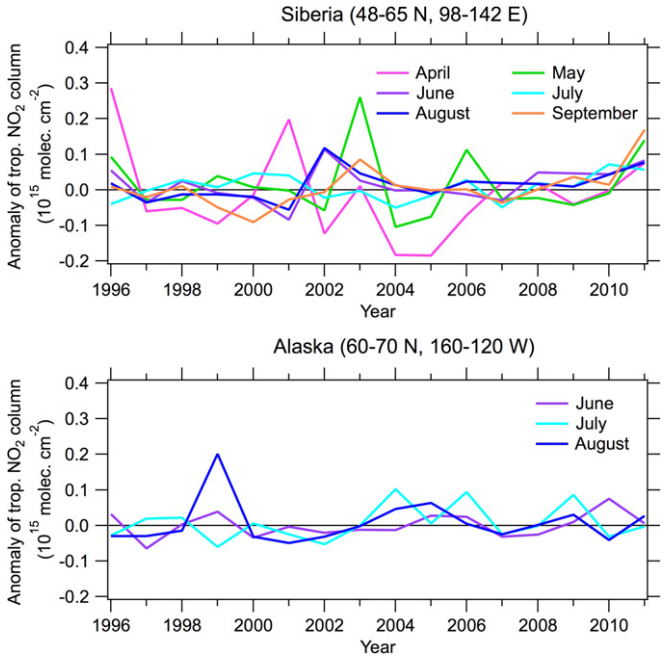

Figure 2. Interannual variability in the regional-mean enhancement of the tropospheric NO_2 column beyond baseline levels over Siberia and Alaska for the period 1996–2011.

The levels of tropospheric NO_2 columns over these boreal regions were low, making the detection of the NO_2 enhancement due to boreal fires challenging. In order to better detect and analyse the enhancements of tropospheric NO_2 columns due to boreal fires, we derived monthly anomalies for Siberia and Alaska by subtracting baseline seasonal cycles as described above. Figure 2 shows interannual variability of the regional-mean enhancement of the tropospheric NO_2 column beyond baseline levels over Siberia and Alaska, for the period 1996–2011. The enhancements are seen to be subtle, but visible, in large-fire years during the summer of 2002, and during the springs of 2003 and 2006 for Siberia. Similarly, enhancements are visible in large-fire years in the summers of 2004, 2005, and 2009 for Alaska.

Figure 3 illustrates the geographical distribution of enhancements of the tropospheric NO_2 column, NO*x* emissions estimated by GFEDv3, and mean FRP as detected by MODIS over Siberia for 2002, 2003, 2006,

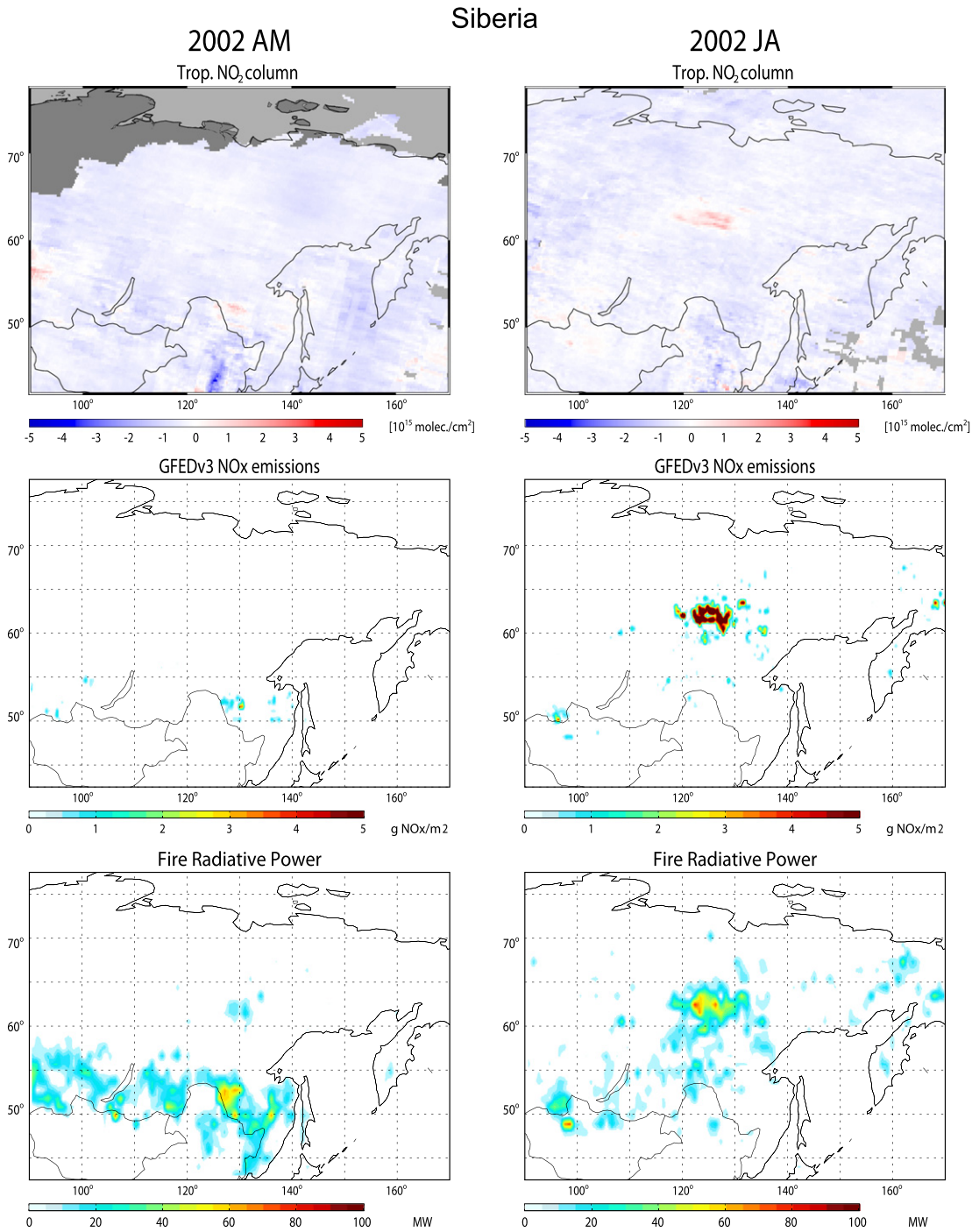

Figure 3. Enhancements of tropospheric NO_2 column (upper panel), NO*x* emissions estimated by GFEDv3 (middle panel), and mean FRP (bottom panel) detected by MODIS over Siberia for 2002, 2003, 2006, and 2008; and over Alaska for 2004, 2005, and 2009. AM, JA, and JJA denote April–May, July–August, and June–July–August, respectively.

and 2008; and over Alaska for 2004, 2005, and 2009. The NO_2 enhancements and mean FRP are temporally averaged, while GFEDv3 NO*x* emissions are totalled over the burning seasons for Siberia and Alaska. While relatively weak in magnitude (on the order of 10^{15} molecules cm^{-2}), significant hot spots of the tropospheric NO_2 enhancements are evident, and the location and intensity of NO_2 enhancements vary depending on the burning event. Fires often occurred East of Lake Baikal in the latitudinal zone of 50–65°N, in far Eastern Siberia. In Alaska, although the horizontal scale of the fires was small compared to Siberia, the NO_2 enhancements can still be seen from GOME and SCIAMACHY retrievals.

For both Siberia and Alaska, locations of NO_2 enhancements are in clear correspondence to those predicted by GFEDv3 and FRP, suggesting that enhancements are attributed to NO*x* emissions from forest fires in Siberia and Alaska. It is interesting to note from a comparison of GFEDv3 estimates with

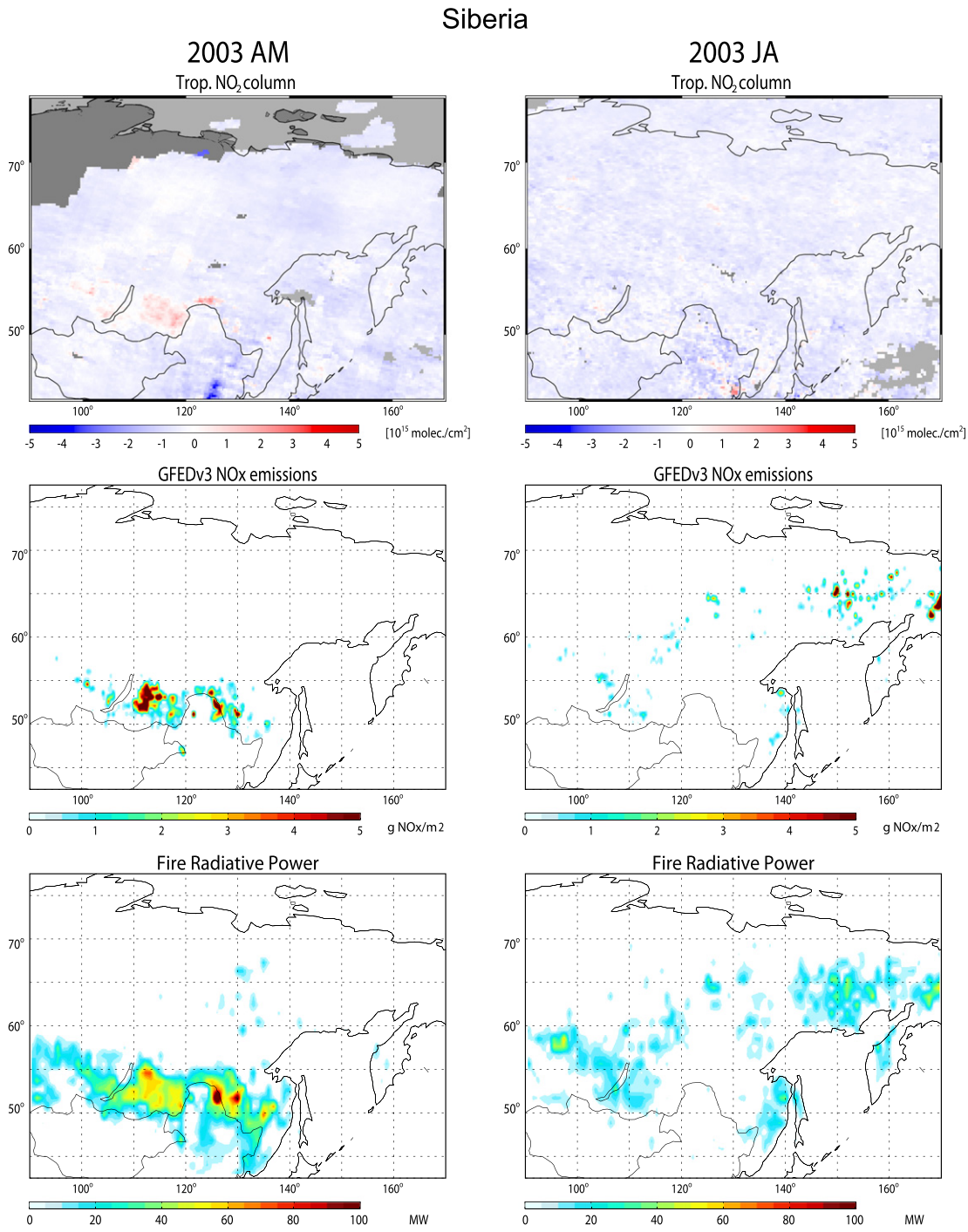

Figure 3. (Continued.)

FRP detections, that there are slight but substantial differences in the location and relative magnitude between these two parameters. For example, in April/May of 2008, GFEDv3 predicted strong emissions around the border between Russia and Mongolia (50–55°N, 120–130°E). So did FRP, but it indicated comparably strong burnings in the West (50–55°N, 110–120°E). In general, the fires indicated by mean FRP cover a large domain than those estimated from GFEDv3. GFEDv3 missed the emissions in Eastern Siberia. The geographical distributions of GFEDv3 emissions rely on the burned area retrieved from MODIS. Hence, these differences would basically reflect the differences between burned scars and FRP.

In order to explore quantitative correspondence of the NO_2 enhancements with GFEDv3 estimates and FRP observations, we examined $1° \times 1°$ grid correlations of the NO_2 enhancements against GFEDv3 NOx emissions and FRP data on a monthly basis. Figure 4 shows examples of the correlations of NO_2 enhancements with FRP and GFEDv3 for Siberia in 2002 and 2006, and for Alaska in 2005. Although the plots are

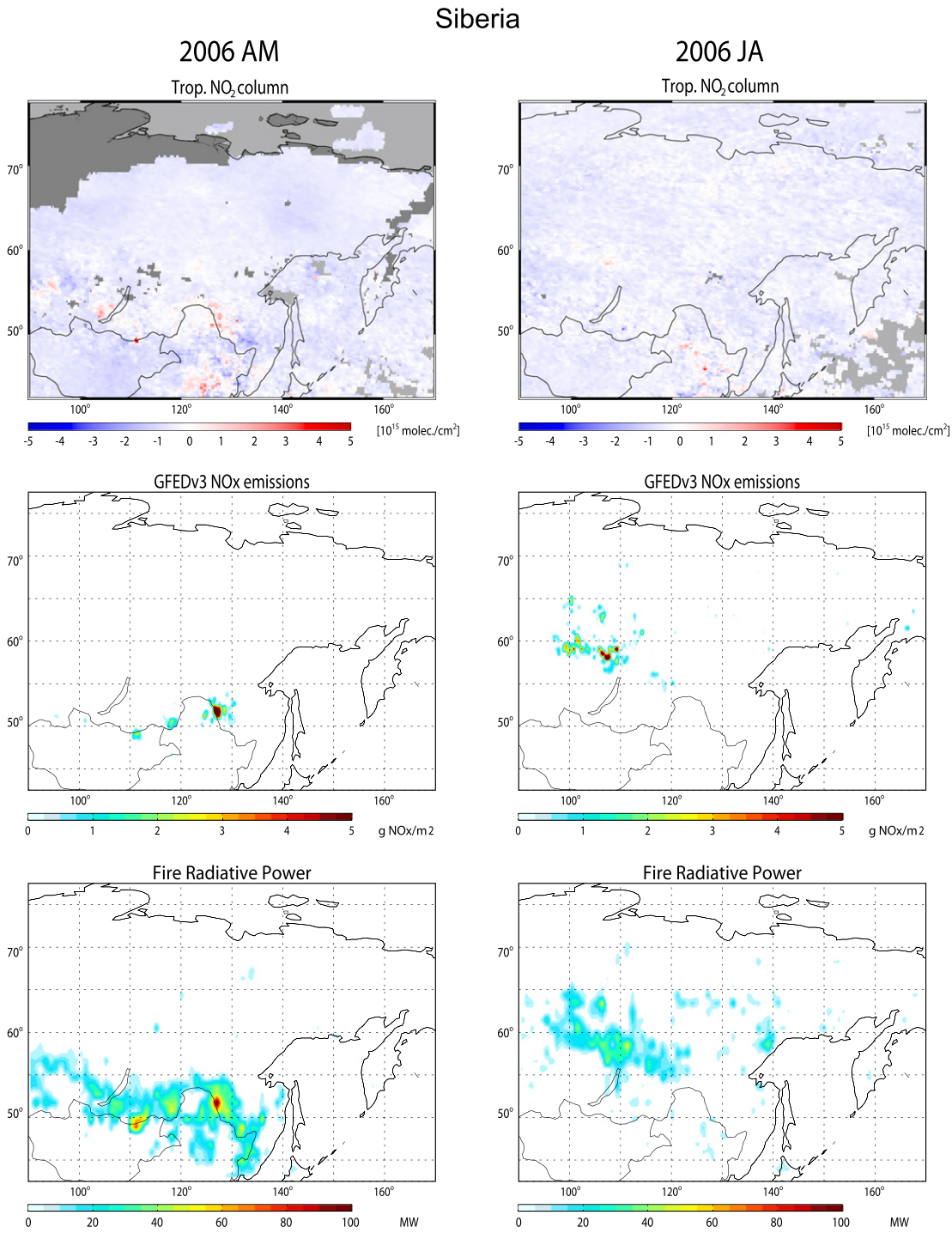

Figure 3. (Continued.)

scattered owing to weak satellite signals, we can see a certain degree of correlation with FRP and GFEDv3, but correlations are much better between the satellite NO_2 retrievals and FRP. For example, in April 2002, GFEDv3 predicts negligible NO*x* emissions, but FRP shows a relatively good correlation with NO_2 enhancements. In general, NO_2 enhancements show a better correlative behaviour with FRP than GFEDv3, suggesting that FRP is a better proxy than burned area for NO*x* emissions from boreal fires. This is reasonable since FRP is thought to be a diagnostic for high-temperature flaming combustion, which oxidizes nitrogen more effectively.

Slopes and determination coefficients (r^2) were calculated for all the $1° \times 1°$ data, and for 10 Mega Watt (MW)-binned data for correlations of tropospheric NO_2 enhancement with FRP. Although in many months the correlations were not statistically significant due to weak signals, statistically significant slopes were found (as indicated by bold numbers in the grey-hatched cells) in 16 out of 66 months for Siberia, and 3 months out of 33 months for Alaska.

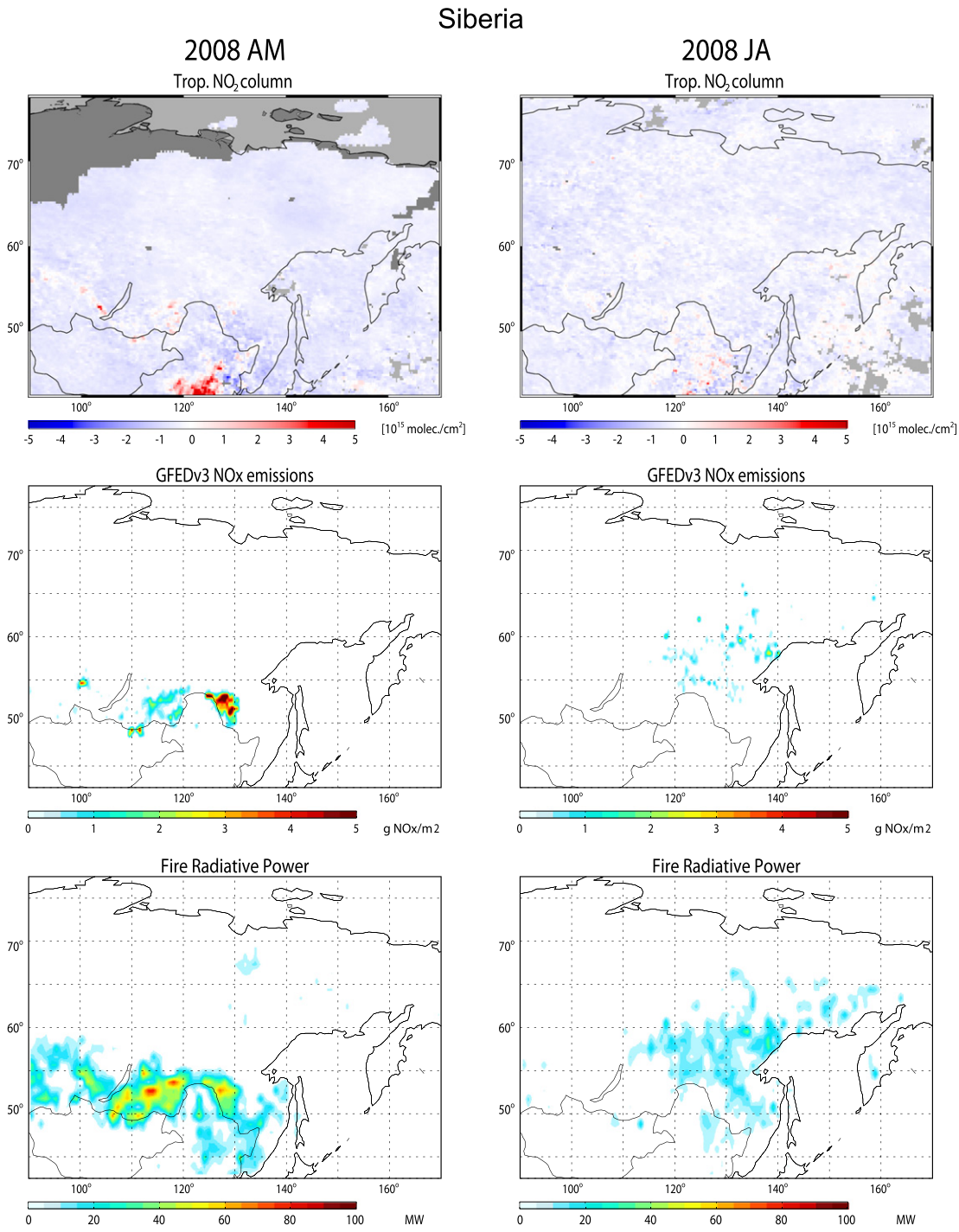

Figure 3. (Continued.)

(Tables S1 and S2 summarize the monthly-based statistics of tropospheric NO_2 enhancement correlations with FRP, for Siberian and Alaskan fires, respectively.) The slopes of tropospheric NO_2 enhancement correlations to FRP are regarded as the enhancement ratio (ER) of the tropospheric NO_2 column due to forest fires (i.e., ΔNO_2 column/ΔFRP). By using the ER, the mass emission coefficient (MEC) of NO*x* emitted from boreal fires can be calculated, following the method devised by the University of Bremen (Schreier *et al* 2014) that converts the NO_2 column number density (in molecules cm^{-2}) as retrieved from satellite instruments, into the column mass concentration (in g cm^{-2}), with the help of Avogadro's number (NA, molecules mol^{-1}), the molar mass (M) of NO (30 g mol^{-1}), and the 1° × 1° grid area (in cm^2), and by assuming a NO_2/NO*x* ratio of 0.75 and a lifetime of NO*x* (in seconds), which we assume to be in the range from 21600 s (6 h) to 7200 s (2 h). The resulting MEC is in the unit of g NO*x* (as NO) MW^{-1} s^{-1}, (or g NO*x* (as NO) MJ^{-1}), because the emissions of NO*x* are reported as NO in the emission inventories for a later

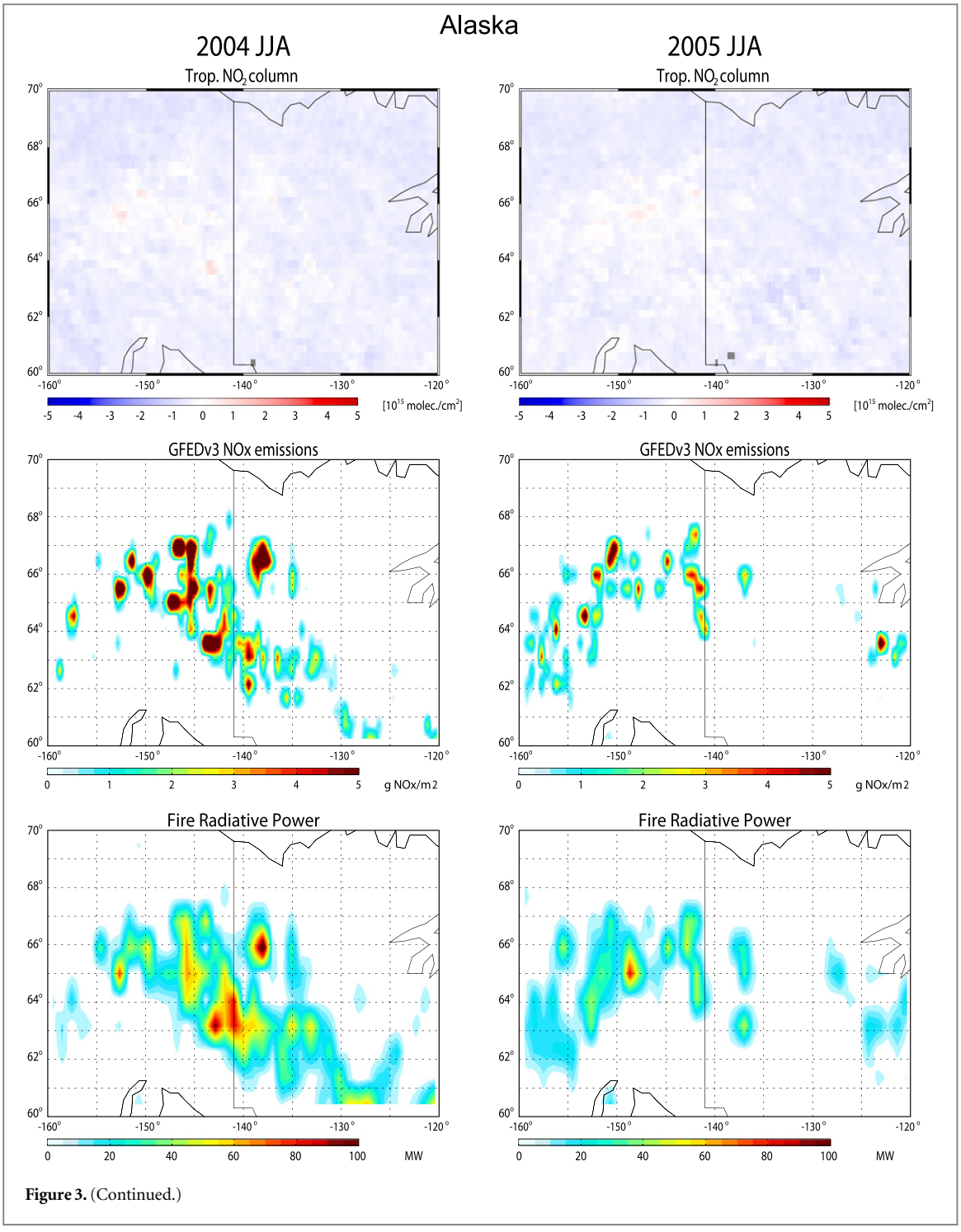

Figure 3. (Continued.)

comparison. In the calculation of the MEC, the ER was used only when: (1) the slopes for both the all- and binned-data were statistically significant; and (2) the determination coefficients (r^2) for binned-data were greater than 0.4. Thresholds for determination coefficients, based on all-data, were relaxed to 0.3 and 0.1 for Siberia and Alaska, respectively, to allow reasonable data selection.

Along with two previous studies by Mebust and Cohen (2014) and Schreier *et al* (2014), the present work examines the relationship of satellite-derived tropospheric NO_2 with FRP, built upon the method first reported for the study of aerosol by Ichoku and Kaufman (2005). Hence, these three studies all apply the same principle, but with minor differences in data and technical processing. The differences include satellite sensors employed (and overpass times), temporal/spatial resolution of the data used, definition of background signals, and NO*x* lifetime assumed. We relied on the satellite observations by GOME and SCIAMACHY, while Mebust and Cohen (2014) relied on those by OMI and Schreier *et al* (2014) used those by both OMI and GOME-2. The local time of the GOME, SCIAMACHY, and GOME-2 observations is

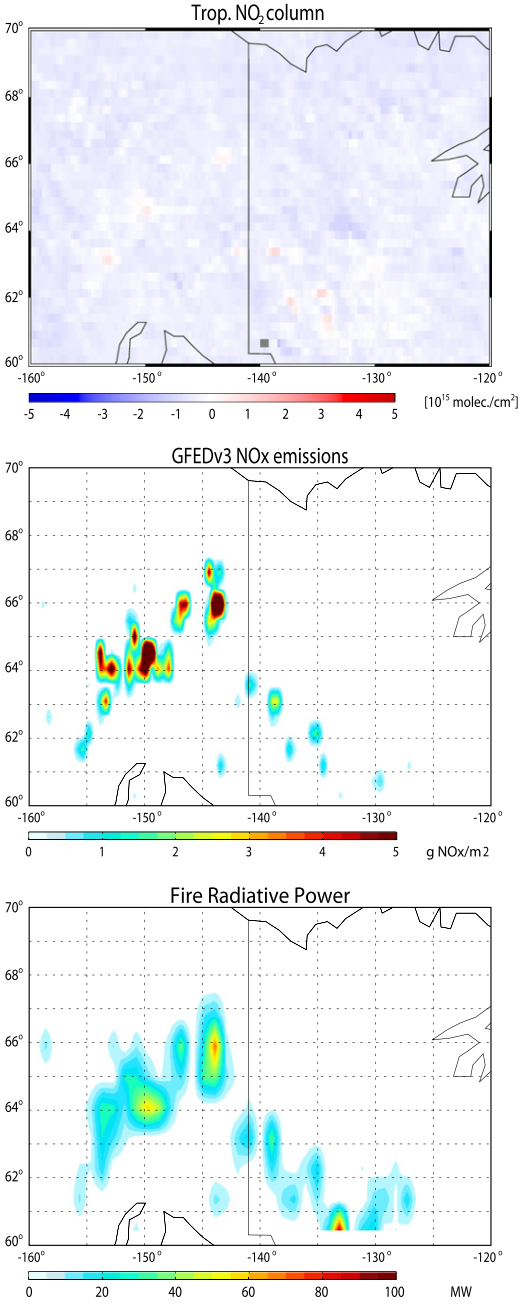

Figure 3. (Continued.)

in the morning, while that of the OMI observations is in the early afternoon. Schreier *et al* (2014) and we used monthly-mean, $1° \times 1°$ gridded data, while Mebust and Cohen (2014) used individual pixels observed by the satellite. The definition of the background NO_2 level is rather different. We used climatological values based on monthly data in low-fire years, and did not use the intercepts from the regressions in figure 4, Mebust and Cohen (2014) used fire-free data at the same location within the a 120 day time window, and Schreier *et al* (2014) used intercepts of the linear regression lines for the regional NO_2-versus-FRP correlations based on monthly data. For the lifetime of NO*x*, we used both 2 and 6 h, as lower and upper limits, respectively, while Schreier *et al* (2014) used for the monthly data a 6 h lifetime based on Beirle *et al* (2011) who examined NO*x* plumes from the megacities, and Mebust and Cohen (2014) chose 2 h based on a quoted range of lifetimes between 2–3 and 7 h from past observations of fire plumes (Yokelson *et al* 1999, Alvarado *et al* 2010). We argue that the NO*x* lifetime could vary from individual fire plumes to monthly averaged fields, with the overall lifetime possibly being longer in monthly fields than in fire plumes. Instantaneous NO_2 lifetimes are generally longer in the morning (e.g, the overpass time at 10:00) than in the afternoon (e.g., the overpass time at 14:30), when chemical regimes are more conducive to fast NO_2 oxidation due to higher temperatures, more dilution, stronger photochemistry. Oxidation chemistry in forest fire plumes can be different from in megacity plumes, and boreal fires occur more often during the summer when photochemistry is faster than in winter. With all these discussions being considered, we conclude that the accuracy of the lifetime assumption is not sufficiently well established yet, and treat a range of possibilities from 2 to 6 h to be equal and as an uncertainty range.

4. Discussion

Table 1 shows a summary of the ER and MEC for Siberia and Alaska. For calculations, data with robust statistical significance (as shown with a bold font in grey-hatched cells in tables S1 and S2) were used. For Siberia, the ER was calculated as $1.58 \pm 1.09 \times 10^{13}$ molecules $cm^{-2}\,MW^{-1}$ ($N = 17$ months) and $1.15 \pm 0.51 \times 10^{13}$ molecules $cm^{-2}\,MW^{-1}$ ($N = 17$ months), for binned- and all- $1° \times 1°$ data, respectively; leading to $1.37 \pm 0.80 \times 10^{13}$ molecules $cm^{-2}\,MW^{-1}$ ($N = 34$ months). Determination of the ER for Alaska was more difficult due to the reduced amount of statistically significant data available. Nevertheless, it was calculated as $0.53 \pm 0.05 \times 10^{13}$ molecules $cm^{-2}\,MW^{-1}$ ($N = 3$ months) and $0.59 \pm 0.18 \times 10^{13}$ molecules $cm^{-2}\,MW^{-1}$ ($N = 3$ months) for binned- and all- $1° \times 1°$ data, respectively, resulting in $0.56 \pm 0.12 \times 10^{13}$ molecules $cm^{-2}\,MW^{-1}$ ($N = 6$ months). The resulting MECs were calculated as 4.21 ± 2.47 for 6 h lifetime (or 12.62 ± 7.40 for 2 h lifetime) and 1.73 ± 0.36 for 6 h lifetime (or 5.18 ± 1.07 for 2 h lifetime) g NO*x* MJ^{-1} (as NO) for Siberia and Alaska, respectively. Although within the range of uncertainty, there was a difference of a factor of 2 in the mean MECs between Siberia and Alaska.

4.1. Comparison of MEC

By using OMI-derived NO_2 data, Mebust and Cohen (2014) determined the MEC of NO*x* from the burning of biomass including that of boreal forest, and by

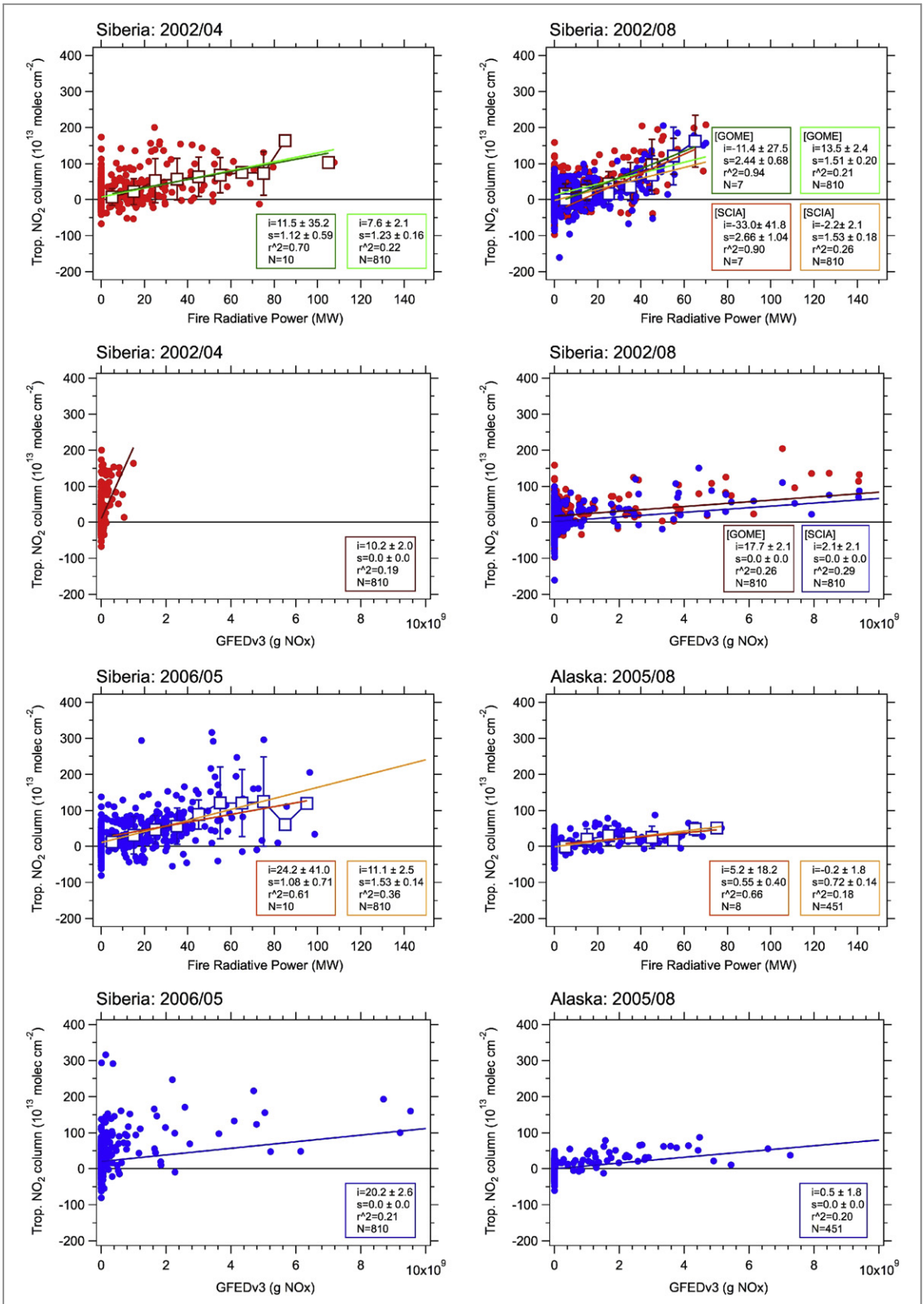

Figure 4. Examples of correlations of tropospheric NO_2 column enhancements with mean FRP observed by MODIS and NO*x* emissions estimates by GFEDv3, for Siberia and Alaska.

assuming a NO*x* lifetime of 2 h the MEC for boreal fires was calculated as 0.250 ± 0.033 g NO*x* MJ^{-1}. They also noted that the MECs were similar in different ecosystem regions regardless of biomes, and were in the range of 0.250–0.362 g NO*x* MJ^{-1}. In contrast, Schreier *et al* (2014) used monthly data from both OMI and GOME-2 observations, assumed a lifetime of 6 h, and reported that MECs varied within a range of 0.28–1.56 g NO*x* MJ^{-1} depending on vegetation types. However, boreal forest was not included in that

Table 1. NO_2 enhancement ratio, NO*x* mass emission coefficient, and NO*x* emission factor for Siberian and Alaskan fires.

Region		Siberia		Alaska	
		Binned data ($r^2 > 0.4$)	All data ($r^2 > 0.3$)	Binned data ($r^2 > 0.4$)	All data ($r^2 > 0.1$)
NO_2 enhancement ratio (10^{13} molecules cm^{-2} MW^{-1})		1.58 ± 1.09 ($N = 17$)	1.15 ± 0.51 ($N = 17$)	0.53 ± 0.05 ($N = 3$)	0.59 ± 0.18 ($N = 3$)
	Average	1.37 ± 0.80 ($N = 34$)		0.56 ± 0.12 ($N = 6$)	
NO*x* mass emission coefficient (g NO*x* MJ^{-1} as NO)		4.21 ± 2.47 (6 h lifetime) 12.62 ± 7.40 (2 h lifetime)		1.73 ± 0.36 (6 h lifetime) 5.18 ± 1.07 (2 h lifetime)	
NO*x* emission factor (g kg^{-1} as NO)	This work	2.71 ± 1.59 (6 h lifetime) 8.14 ± 4.78 (2 h lifetime)		1.11 ± 0.23 (6 h lifetime) 3.34 ± 0.69 (2 h lifetime)	
	Akagi *et al* (2011)	0.90 ± 0.69 (for boreal forest); 1.12 ± 0.69 (for extratropical forest)			
	Andreae and Merlet (2001)	3.0 ± 1.4 (for extratropical forest)			

analysis. Therefore, substantial discrepancies exist between past satellite-based studies, and these are likely related to the inherently varying lifetimes of NO*x* in individual fire plumes, the diurnal variability of emissions, and the chemical transformation of NO*x*.

As mentioned above, there are some differences among the three approaches. If the large-fire years resulted in higher background levels than the small-fire years that we adopted as the background, this could be a possible source of uncertainty. However, since the differences in the background levels between large- and small-fire years were usually negligible (within ±10%, at most), this does not constitute a source of error. As seen above, differences by a factor of 3 in the NO*x* lifetime assumption (6 versus 2 h) can greatly affect the MEC estimates. Another source of the uncertainty is the use of monthly data that involves a number of averaging steps, resulting in weak relationships between the FRP and tropospheric NO_2, compared to the correlations on a daily basis.

The values of MECs reported in this study, of 1.7–4.2 (with 6 h lifetime) and 5.2–12.6 (with 2 h lifetime) g NO*x* MJ^{-1}, appear high compared to those in the previous two studies. However, past studies yielded climatological MECs, and we used large-fire data (data with robust statistical significance, even for monthly means, as shown in tables S1 and S2), which would result in higher values. It is understood that there is a natural variability in the values of MECs, depending on burning, climate, and fuel conditions in individual fires, and the MECs observed in this study seem within a reasonable range of this natural variability. In order to obtain rough estimates of 'climatological' MECs by our approach, we considered all the monthly-based statistics from the tropospheric NO_2-versus-FRP correlations (regardless of statistical significance in tables S1 and S2). The calculated 'climatological' MECs fell into the range of 0.4–1.7 (with 6 h lifetime) and 1.2–4.9 (with 2 h lifetime) g NO*x* MJ^{-1} as NO. We see an improved agreement, in particular with Schreier *et al* (2014) who provided climatological estimates by using monthly data with the assumption of a 6 h lifetime. It seems that this can explain a substantial portion (60–80%) of the discrepancy between our work and past estimates.

4.2. Comparison of EFs

In this section, we derive EF from the MEC, make a comparison with previous estimates, and discuss the degree of agreement. Previous efforts to determine EFs, based on *in situ* observations and burning experiments, are well summarized in the comprehensive reviews of Andreae and Merlet (2001) and Akagi *et al* (2011). It should be noted that, for some species from some sources, EFs are calculated based only on a handful of available measurements; hence, the reported EFs are not necessarily robust and need to be continuously evaluated. For example in Akagi *et al* (2011), the EF of NO*x* from boreal fires was calculated from one ground-based measurement and three airborne measurements in North America. It should also be noted that the EFs for boreal fires in these reviews are biased to North American fires, since the raw data was mostly collected in North America. Furthermore, EFs can greatly vary depending on the burning conditions (flaming to smoldering), availability of air and humidity, and the type of fuel involved. For example, emissions of CO_2 and NO*x* are predominant in flaming conditions, while those of CO and NMVOCs predominate in smoldering. For short-lived species including NO*x*, the age of air samples observed is also important in determination of EFs, as demonstrated by Kudo *et al* (2014) who showed the rapid loss of alkenes in fire plumes even within a few hours. Without appropriate correction by air mass age therefore, EFs would be greatly underestimated.

In order to convert MECs to EFs, a conversion factor (CF) from FRP to dry biomass burned is required. Based on ground-based experiments linking direct FRP observations to biomass consumption for small-scale fires, Wooster *et al* (2005) proposed a universal CF of 0.368 kg MJ^{-1} for the conversion from FRP to dry matter burned. A similar value of 0.41 kg MJ^{-1} was

proposed by Vermote *et al* (2009). In a comparison of the dry matter combustion rate of FRP and GFEDv3, Heil *et al* (2010) found that the FRP-dry matter burned CF depended on the land cover type. Kaiser *et al* (2012) determined land-cover dependent CF for eight land cover classes, where the CF for boreal fires (extratropical forest with organic soil by their definition) was 1.55 kg MJ^{-1}. Therefore, in recognition that there is a substantial range (approximately ± 60%) in CF estimates, we adopt the CF of 1.55 kg MJ^{-1} from Kaiser *et al* (2012) to calculate the EFs in our analysis, since boreal forest has a huge pool of biomass at ground-level or below-ground (e.g., peat) which is a major source of fuel (not the leaves and trunk). The resulting EFs for Siberian and Alaskan fires are therefore 2.71 ± 1.59 and 1.11 ± 0.23 g kg^{-1}, respectively, for the NO*x* lifetime of 6 h. For the NO*x* lifetime of 2 h, the EFs are 8.14 ± 4.78 and 3.34 ± 0.69 g kg^{-1}, respectively. Possible explanation would be higher fire intensity (e.g., more flaming) and/or more availability of peat-like biomass in Siberia than Alaska.

Akagi *et al* (2011) reported the EF of NO*x* explicitly for boreal forest fires as 0.90 ± 0.69 g NO*x* kg^{-1} dry biomass as NO. Alvarado *et al* (2010) derived an NO*x* EF of 1.06 g NO*x* kg^{-1} dry biomass for Canadian fire plumes. Andreae and Merlet (2001) reported EFs of NO*x* for extratropical forest fires as 3.0 ± 1.4 g NO*x* kg^{-1}. Since extratropical forest is comprised of boreal and temperate forest, Akagi *et al* (2011) gave a greater weight to boreal forest fire EF than temperate forest fire EF (2.51 ± 1.02), with a ratio of 87:13 (based on relative global fuel consumption), to generate their extratropical EF of 1.12 ± 0.69 g NO*x* kg^{-1}. Hence, at a maximum there is roughly a factor difference of 3 between these two inventories. Akagi *et al* (2011) noted that their total EFs for boreal fires reflected a large component of smoldering combustion data, suggesting that the EF of NO*x* for boreal fires was dominantly calculated by smoldering burning, which releases much less NO*x* emissions than flaming burning. Smoldering is not always dominant as there is evidence of pyro-convective fires over boreal forest (Fromm and Servranckx 2003). Therefore, the true EF of NO*x* from boreal fires would be in the range of 1–3 g NO*x* kg^{-1}, and the above-derived satellite-based values of 1.1–8.1 partly overlap with this range. While the advantage of satellite-based analysis is that it enables statistical robustness due to the huge number of data, the associated uncertainty is high compared to *in situ* measurements used to determine EFs in the previous reviews. It is therefore considered that both *in situ* measurement- and satellite-based approaches should be used in tandem to further test our understanding of EFs, and to narrow down the uncertainty of estimates.

Acknowledgments

We thank Krishna P Vadrevu for valuable discussion on fire intensity, and Kimiko Suto, Haruka Yamagishi, and Edit Nagy-Tanaka for technical support. We acknowledge the tropospheric NO_2 column data from the GOME and SCIAMACHY sensors available at www.temis.nl. We also thank NASA for providing MODIS fire radiative power data. The Giovanni online data system, developed and maintained by NASA GES DISC, was utilized. Data of GFED were obtained at http://globalfiredata.org. This work was supported by the Environmental Research and Technology Development Fund (2-1505) of the Ministry of the Environment, Japan. The authors thank three reviewers for their comments for improving the paper.

References

Akagi S K, Yokelson R J, Wiedinmyer C, Alvarado M J, Reid J S, Karl T, Crounse J D and Wennberg P O 2011 Emission factors for open and domestic biomass burning for use in atmospheric models *Atmos. Chem. Phys.* **11** 4039–72

Alvarado M J *et al* 2010 Nitrogen oxides and PAN in plumes from boreal fires during ARCTAS-B and their impact on ozone: an integrated analysis of aircraft and satellite observations *Atmos. Chem. Phys.* **10** 9739–60

Andreae M O and Merlet P 2001 Emission of trace gases and aerosols from biomass burning *Glob. Biogeochem. Cycles* **15** 955–66

Beirle S, Boersma K F, Platt U, Lawrence M G and Wagner T 2011 Megacity emissions and lifetimes of nitrogen oxides probed from space *Science* **333** 1737–9

Boersma K F, Eskes H J and Brinksma E J 2004 Error analysis for tropospheric NO_2 retrieval from space *J. Geophys. Res.* **109** D04311

Boersma K F *et al* 2011 An improved tropospheric NO_2 column retrieval algorithm for the Ozone Monitoring Instrument *Atmos. Meas. Tech.* **4** 1905–28

Castellanos P and Boersma K F 2012 Reductions in nitrogen oxides over Europe driven by environmental policy and economic recession *Sci. Rep.* **2** 265

Castellanos P, Boersma K F and van der Werf G R 2014 Satellite observations indicate substantial spatiotemporal variability in biomass burning NO*x* emission factors for South America *Atmos. Chem. Phys.* **14** 3929–43

Fromm M and Servranckx R 2003 Transport of forest fire smoke above the tropopause by supercell convection *Geophys. Res. Lett.* **30** 1542

Ghude S D, Fadnavis S, Beig G, Polade S D and van der A R J 2008 Detection of surface emission hot spots, trends, and seasonal cycle from satellite-retrieved NO_2 over India *J. Geophys. Res.* **113** D20305

Ghude S D, Lal D M, Beig G, van der A R and Sable D 2010 Rain-induced soil NO*x* emission from india during the onset of the summer monsoon: a satellite perspective *J. Geophys. Res.* **115** D16304

Heil A, Kaiser J W, van der Werf G R, Wooster M J, Schultz M G and Dernier van der Gon H 2010 *Assessment of the Real-Time Fire Emissions (GFASv0) by MACC Tech. Memo.* 628 ECMWF, Reading, UK

Hilboll A, Richter A and Burrows J P 2013 Long-term changes of tropospheric NO_2 over megacities derived from multiple satellite instruments *Atmos. Chem. Phys.* **13** 4145–69

Hudman R C, Russell A R, Valin L C and Cohen R C 2010 Interannual variability in soil nitric oxide emissions over the United States as viewed from space *Atmos. Chem. Phys.* **10** 9943–52

Huijnen V et al 2012 Hindcast experiments of tropospheric composition during the summer 2010 fires over Western Russia Atmos. Chem. Phys. 12 4341–64
Ichoku C and Kaufman Y J 2005 A method to derive smoke emission rates from MODIS fire radiative energy measurements IEEE Trans. Geosci. Remote Sens. 43 2636–49
Jaffe D, Bertschi I, Jaeglé L, Novelli P, Reid J S, Tanimoto H, Vingarzan R and Westphal D L 2004 Long-range transport of Siberian biomass burning emissions and impact on surface ozone in Western North America Geophys. Res. Lett. 31 L16106
Jaffe D A and Wigder N L 2012 Ozone production from wildfires: a critical review Atmos. Environ. 51 1–10
Justice C O et al 2002 The MODIS fire products Remote Sens. Environ. 83 244–62
Kaiser J W et al 2012 Biomass burning emissions estimated with a global fire assimilation system based on observed fire radiative power Biogeosciences 9 527–54
Kaufman Y J, Justice C O, Flynn L P, Kendall J D, Prins E M, Giglio L, Ward D E, Menzel W P and Setzer A W 1998 Potential global fire monitoring from EOS-MODIS J. Geophys. Res. Atmos. 103 32215–38
Kudo S et al 2014 Emissions of nonmethane volatile organic compounds from open crop residue burning in the Yangtze River Delta region, China J. Geophys. Res. Atmos. 119 7684–98
Mebust A K and Cohen R C 2014 Space-based observations of fire NOx emission coefficients: a global biome-scale comparison Atmos. Chem. Phys. 14 2509–24
Mebust A K, Russell A R, Hudman R C, Valin L C and Cohen R C 2011 Characterization of wildfire NOx emissions using MODIS fire radiative power and OMI tropospheric NO_2 columns Atmos. Chem. Phys. 11 5839–51
Miyazaki K, Eskes H J and Sudo K 2012 Global NOx emission estimates derived from an assimilation of OMI tropospheric NO_2 columns Atmos. Chem. Phys. 12 2263–88
Richter A, Burrows J P, Nu¨ß H, Granier C and Niemeier U 2005 Increase in tropospheric nitrogen dioxide over China observed from space Nature 437 129–32
Schreier S F, Richter A, Kaiser J W and Burrows J P 2014 The empirical relationship between satellite-derived tropospheric NO_2 and fire radiative power and possible implications for fire emission rates of NOx Atmos. Chem. Phys. 14 2447–66
Tanimoto H 2009 Increase in springtime tropospheric ozone at a mountainous site in Japan for the period 1998–2006 Atmos. Environ. 43 1358–63
Tanimoto H, Kajii Y, Hirokawa J, Akimoto H and Minko N P 2000 The atmospheric impact of boreal forest fires in far Eastern Siberia on the seasonal variation of carbon monoxide: observations at Rishiri, a Northern remote island in Japan Geophys. Res. Lett. 27 4073–6
Tanimoto H, Matsumoto K and Uematsu M 2008 Ozone–CO correlations in Siberian wildfire plumes observed at Rishiri Island SOLA 4 65–8
Tanimoto H et al 2009 Exploring CO pollution episodes observed at Rishiri Island by chemical weather simulations and AIRS satellite measurements: long-range transport of burning plumes and implications for emissions inventories Tellus B 61B 394–407
Turquety S et al 2007 Inventory of boreal fire emissions for North America in 2004: importance of peat burning and pyroconvective injection J. Geophys. Res. 112 D12S03
van der A R J, Eskes H J, Boersma K F, van Noije T P C, Van Roozendael M, De Smedt I, Peters D H M U and Meijer E W 2008 Trends, seasonal variability and dominant NOx source derived from a ten year record of NO_2 measured from space J. Geophys. Res. 113 D04302
Vermote E, Ellicott E, Dubovik O, Lapyonok T, Chin M, Giglio L and Roberts G J 2009 An approach to estimate global biomass burning emissions of organic and black carbon from MODIS fire radiative power J. Geophys. Res. 114 D18205
van der Werf G R, Randerson J T, Giglio L, Collatz G J, Mu M, Kasibhatla P S, Morton D C, DeFries R S, Jin Y and van Leeuwen T T 2010 Global fire emissions and the contribution of deforestation, savanna, forest, agricultural, and peat fires (1997–2009) Atmos. Chem. Phys. 10 11707–35
van Leeuwen T T and van der Werf G R 2011 Spatial and temporal variability in the ratio of trace gases emitted from biomass burning Atmos. Chem. Phys. 11 3611–29
Wooster M J, Roberts G, Perry G L W and Kaufman Y J 2005 Retrieval of biomass combustion rates and totals from fire radiative power observations: FRP derivation and calibration relationships between biomass consumption and fire radiative energy release J. Geophys. Res. 110 D24311
Yokelson R J, Goode J G, Ward D E, Susott R A, Babbitt R E, Wade D D, Bertschi I, Griffith D W T and Hao W M 1999 Emissions of formaldehyde, acetic acid, methanol, and other trace gases from biomass fires in North Carolina measured by airborne Fourier transform infrared spectroscopy J. Geophys. Res. 104 30109–25
Yurganov L N et al 2004 A quantitative assessment of the 1998 carbon monoxide emission anomaly in the Northern Hemisphere based on total column and surface concentration measurements J. Geophys. Res. 109 D15305
Yurganov L N et al 2005 Increased Northern Hemispheric carbon monoxide burden in the troposphere in 2002 and 2003 detected from the ground and from space Atmos. Chem. Phys. 5 563–73
Yurganov L, McMillan W, Grechko E and Dzhola A 2010 Analysis of global and regional CO burdens measured from space between 2000 and 2009 and validated by ground-based solar tracking spectrometers Atmos. Chem. Phys. 10 3479–94